On localization of Dirac fermions by disorder

Medvedyeva, M.V.

Chapter 1

Introduction

1.1 Preface

Nonrelativistic quantum mechanics is based on the Schrödinger equation, which describes particles with a quadratic dependence of energy on momentum. Conduction electrons in metals and semiconductors follow this equation. The effective mass is different from the free electron mass, due to the effect of the lattice potential, but it does not vanish.

In recent years materials were discovered in which the energy of excitations near the Fermi level depends linearly rather than quadratically on momentum. This is the same linear dispersion relation as for photons, so these materials mimic the dynamics of massless relativistic particles (although the Fermi velocity is much less than the speed of light). The excitations could be electrons or holes in a carbon monolayer (graphene), or they could be neutral quasiparticle excitations in an unconventional superconductor (with p-wave or d-wave symmetry of the order parameter).

The massless excitations are called Dirac fermions, because they satisfy a Dirac equation rather than a Schrödinger equation. The Dirac equation was studied extensively in the context of relativistic quantum mechanics, but questions related to the effect of disorder did not play a role in that context. These effects are, however, central to the behavior of Dirac fermions in condensed matter.

Localization is a purely quantum mechanical effect of disorder, discovered by P.W. Anderson in 1958 [7]. Interference prevents the spreading of a wave packet, turning a metal into an insulator. This effect is now

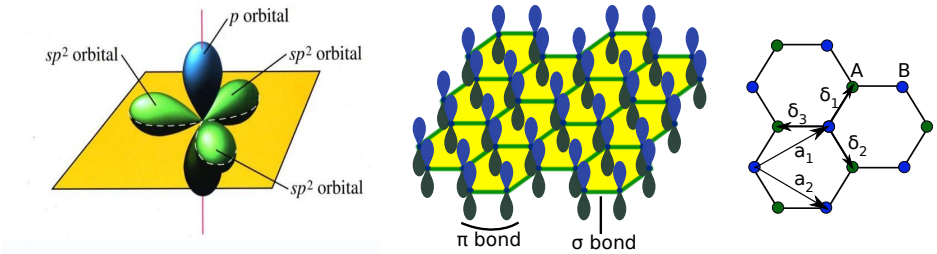

Figure 1.1. The left panel shows the sp^2-hybridized orbitals of a carbon atom, the central panel shows their arrangement in a honeycomb lattice known as graphene. The right panel shows the A and B sublattices that form the honeycomb lattice, with lattice vectors $\boldsymbol{a}_1$, $\boldsymbol{a}_2$ and nearest neighbor vectors $\boldsymbol{\delta}_1$, $\boldsymbol{\delta}_2$, $\boldsymbol{\delta}_3$. From Ref. [22].

well understood, both by an intuitive scaling theory [1] and by field theoretical approaches [125]. It has been tested by numerical simulations [65] and by experiments [37].

These studies considered massive electrons, starting from the Schrödinger equation. Localization of massless Dirac fermions is qualitatively different. Some aspects of the localization of Dirac fermions are studied in this thesis.

In this introductory chapter we present background material, and an outline of the following chapters. We start by introducing the physical realizations of Dirac fermions that we will be considering.

1.2 Dirac fermions in graphene

1.2.1 Gapless graphene

Graphene is a monolayer of graphite. The atomic configuration of the carbon atoms is $1s^2 2s^2 2p^2$, in graphene their electronic configuration is $1s^2 2s 2p^3$. Due to sp^2-hybridization the atoms form a hexagonal lattice (σ-bonds), see Fig. 1.1. The p_z orbitals do not participate in the hybridization (π-bond). Electrical conduction is due to hopping between the p_z orbitals.

The unit cell of the hexagonal lattice consists of two atoms, which form the A and B sublattices. The tight-binding model with nearest

neighbor hopping only couples different sublattices, corresponding to the off-diagonal blocks in the Hamiltonian

$$\mathcal{H} = \begin{pmatrix} 0 & t^* \sum_{j=1,2,3} \exp(-i\boldsymbol{k}\cdot\boldsymbol{\delta}_j) \\ t \sum_{j=1,2,3} \exp(i\boldsymbol{k}\cdot\boldsymbol{\delta}_j) & 0 \end{pmatrix}. \tag{1.1}$$

The $\boldsymbol{\delta}_j$'s are three nearest neighbor vectors,

$$\boldsymbol{\delta}_1 = \frac{a}{2}(1,\sqrt{3}), \quad \boldsymbol{\delta}_2 = \frac{a}{2}(1,-\sqrt{3}), \quad \boldsymbol{\delta}_3 = a(1,0),$$

$a \approx 1.42$ Å is the lattice constant, and $t \approx 2.8$ eV is the nearest neighbor hopping energy.

The Hamiltonian (1.1) has energy bands $E(\boldsymbol{k})$ given by

$$E = \pm t\sqrt{3 + 2\cos\sqrt{3}k_y a + 4\cos\frac{\sqrt{3}k_y a}{2}\cos\frac{3k_x a}{2}}. \tag{1.2}$$

At the points

$$K = \left(\frac{2\pi}{3a}, \frac{2\pi}{3\sqrt{3}a}\right), \quad K' = \left(\frac{2\pi}{3a}, -\frac{2\pi}{3\sqrt{3}a}\right)$$

the gap in the spectrum is closed. Near these two socalled Dirac points the energy-momentum relation is linear.

Linearization of the tight-binding Hamiltonian near a Dirac point gives the two-dimensional massless Dirac Hamiltonian,

$$\mathcal{H} = \hbar v_F \begin{pmatrix} 0 & \delta k_x \mp i\delta k_y \\ \delta k_x \pm i\delta k_y & 0 \end{pmatrix}, \tag{1.3}$$

which can be written more compactly in terms of Pauli matrices,

$$\mathcal{H} = \hbar v_F(\sigma_x \delta k_x \pm \sigma_y \delta k_y). \tag{1.4}$$

The wave vector $\delta\boldsymbol{k}$ is measured relative to point K (upper sign) or relative to point K' (lower sign). The Fermi velocity v_F is expressed through the parameters of the lattice as $v_F = 3at/2 \approx 10^6$ m/s. This is relatively large, but still much smaller than the speed of light, so the dynamics only mimics that of relativistic particles.

The literature on graphene has exploded, since the first isolation of carbon monolayers in 2004 by A. K. Geim and K. S. Novoselov with their group (recently honored by a Nobel prize). We refer to a comprehensive review [22] for references.

1.2.2 Gapped graphene

The relatively large Fermi velocity in graphene is promising for transistor applications, but the absence of a band gap is a complication: It is impossible to completely switch off the conductivity. A band gap is represented by an additional term $mv_F^2\sigma_z$ in Dirac equation, which in the relativistic analogue would correspond to a mass term,

$$\mathcal{H} = mv_F^2\sigma_z + \hbar v_F(\sigma_x\delta k_x \pm \sigma_y\delta k_y). \tag{1.5}$$

The physical meaning of this term is a potential which takes on different values on the two sublattices. Such a staggered potential can be imposed on graphene in different ways, for example, by chemisorption of atoms to the π-bonds or by a substrate.

Let us consider the first possibility in some more detail [27]. We assume that the adatom deposited on graphene forms a covalent bond with a particular carbon atom (fluorine, hydrogen, or hedroxyl groups are known to act like this). Then the sublattice symmetry is locally broken. In general the concentration of adatoms on the two sublattices is almost equivalent. But spontaneous sublattice symmetry breaking can happen if it is energetically more favorable for adatoms to be on the same sublattice. Namely, each adsorbent locally changes the electronic density and interacts via this change of electronic density with another adatom, in such a way that the interaction depends on which sublattice the adatom is placed.

If the configuration with adatoms on the same sublattice has lower energy than with adatoms on different sublattices, then domains with broken sublattice symmetry are generated. This can happen if the adatoms may move along the flake, which requires that the activation barrier is smaller than the desorption barrier. This condition is not met for hydrogen adatoms, but it can be valid for other adatoms, for example the halogens.

Turning to the second possibility, there are substrates for graphene which break the sublattice symmetry [46, 130], for example SiC or BN. Such substrates have a hexagonal lattice structure and almost the same lattice constant as graphene. The onsite potentials are different for each sublattice, due to different atoms on the sublattices, see Fig. 1.2. If the graphene lattice is matched with the substrate lattice, then the sublattice symmetry is broken, which leads to a band gap (estimated in Ref. [46] at 53 meV for BN).

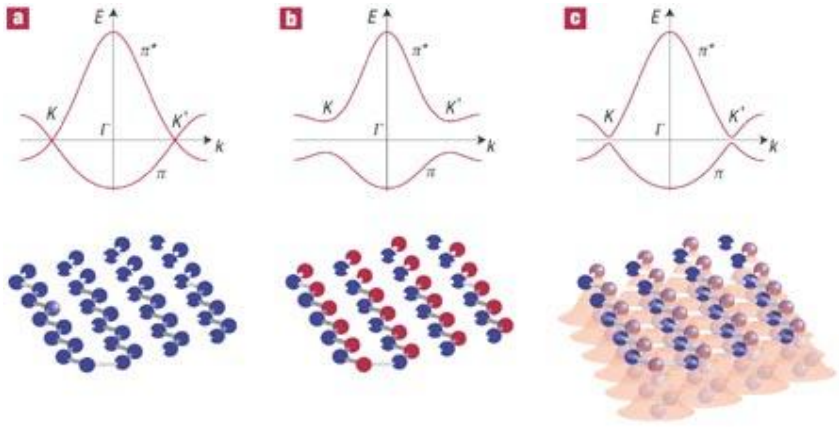

Figure 1.2. Schematic representation of crystal structure and dispersion relation: a) free-standing graphene; b) boron-nitride, BN (with different atoms represented by different colours); c) graphene on BN. As different atoms of the substrate have different potentials, the sublattice symmetry is broken and a gap is opened. From Ref. [89].

1.3 Dirac fermions in superconductors

In conventional superconductors an electron with spin up, momentum $\boldsymbol{k}$ forms a Cooper pair with an electron with spin down, momentum $-\boldsymbol{k}$. This spin-singlet, s-wave pairing is isotropic both with respect to the spin and with respect to the orbital degree of freedom. Superconductors with anisotropic pairing are called unconventional. The high-T_c cuprate superconductors are a notable example, where the Cooper pairs have spin singlet, d-wave symmetry. Spin-triplet, p-wave pairing appears in strontium ruthenate (Sr_2RuO_4). Quasiparticle excitations in these superconductors are Dirac fermions, as we will discuss in this section.

1.3.1 Pairing symmetry

Let us first classify the types of electron pairing, consistent with the requirement of an antisymmetric wave function. The wave function of two electrons consists of a spin part χ and orbital part Δ (also called the pair potential). The full wave function should be antisymmetric with respect to interchange of the two fermions: $\Delta(\boldsymbol{k})\chi_{12} = -\Delta(-\boldsymbol{k})\chi_{21}$, with $\boldsymbol{k}$ the momentum of the relative motion of the electron pair.

The spin state is given in terms of the Pauli matrices

$$\sigma_x = \begin{pmatrix} 0 & 1 \\ 1 & 0 \end{pmatrix}, \ \sigma_y = \begin{pmatrix} 0 & -i \\ i & 0 \end{pmatrix}, \ \sigma_z = \begin{pmatrix} 1 & 0 \\ 0 & -1 \end{pmatrix}. \tag{1.6}$$

The basis states for a single spin are the spinors

$$|\uparrow\rangle = \begin{pmatrix} 1 \\ 0 \end{pmatrix}, \ |\downarrow\rangle = \begin{pmatrix} 0 \\ 1 \end{pmatrix}. \tag{1.7}$$

The basis states for two spins are

$$|\uparrow\uparrow\rangle = \begin{pmatrix} 1 & 0 \\ 0 & 0 \end{pmatrix}, \ |\uparrow\downarrow\rangle = \begin{pmatrix} 0 & 1 \\ 0 & 0 \end{pmatrix}, \ |\downarrow\uparrow\rangle = \begin{pmatrix} 0 & 0 \\ 1 & 0 \end{pmatrix}, \ |\downarrow\downarrow\rangle = \begin{pmatrix} 0 & 0 \\ 0 & 1 \end{pmatrix}. \tag{1.8}$$

The spin-singlet state is given by

$$|\uparrow\downarrow\rangle - |\downarrow\uparrow\rangle = \begin{pmatrix} 0 & 1 \\ -1 & 0 \end{pmatrix} = i\sigma_y, \tag{1.9}$$

which is antisymmetric with respect to interchange of the particles. Hence for spin-singlet superconductivity the Cooper pair wave function is

$$\Psi = \Delta(\boldsymbol{k}) i\sigma_y, \tag{1.10}$$

with $\Delta(-\boldsymbol{k}) = \Delta(\boldsymbol{k})$.

For s-wave pairing the pair potential $\Delta = \Delta_0$ is a constant. The superconducting gap is then isotropic, equal to Δ_0. For d-wave pairing one has an anisotropic pair potential,

$$\Delta(\boldsymbol{k}) = (\Delta_0/k_F^2)(k_x^2 - k_y^2). \tag{1.11}$$

The gap in this case vanishes along the nodal lines $|k_x| = |k_y|$.

Spin-triplet pairing is described by the wave function

$$\Psi = \Delta_{\uparrow\uparrow}(\boldsymbol{k}) \ |\uparrow\uparrow\rangle + \Delta_{\uparrow\downarrow}(\boldsymbol{k})(|\uparrow\downarrow\rangle + |\downarrow\uparrow\rangle) + \Delta_{\downarrow\downarrow}(\boldsymbol{k}) \ |\downarrow\downarrow\rangle. \tag{1.12}$$

An equivalent representation is in terms of the three-dimensional vector $\boldsymbol{d}(\boldsymbol{k})$ and the vector of Pauli matrices $\boldsymbol{\sigma}$,

$$\Psi = i(\boldsymbol{d} \cdot \boldsymbol{\sigma})\sigma_y = \begin{pmatrix} -d_x + id_y & d_z \\ d_z & d_x + id_y \end{pmatrix}. \tag{1.13}$$

For p-wave pairing the function $\boldsymbol{d}(\boldsymbol{k})$ is linear in $\boldsymbol{k}$. In Sr_2RuO_4 it has the form [57]

$$\boldsymbol{d}(\boldsymbol{k}) = (\Delta_0/k_F)(k_x \pm ik_y)\boldsymbol{d}_0. \tag{1.14}$$

This state breaks time-reversal symmetry (by choosing the sign $\pm$). It is called a chiral p-wave state.

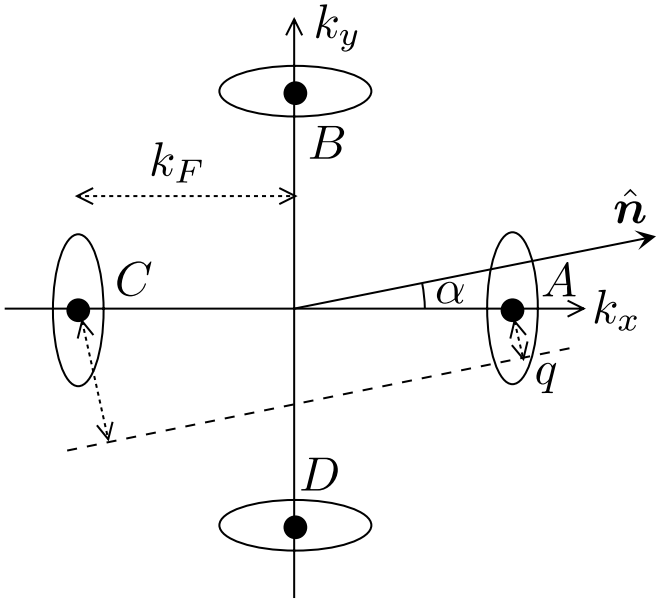

Figure 1.3. Ellipsoidal equal-energy contours of low-energy excitations in the Brillouin zone of superconductor with d_{xy} symmetry. The contours are centered at the four nodal points (solid dots), where the order parameter vanishes on the Fermi surface. From Ref. [9].

1.3.2 Dirac fermions in *d*-wave superconductors

In the vicinity of the nodal lines (where the pair potential (1.11) vanishes) the Hamiltonian for the quasiparticle excitations can be linearized, resulting in a Dirac Hamiltonian, see Fig. 1.3.

To see how this works out, we start from a tight-binding Hamiltonian in second quantization,

$$H = \sum_{ij} (c^\dagger_{i\uparrow}, c_{i\downarrow}) \begin{pmatrix} t_{ij} - \mu\delta_{ij} & \Delta_{ij} \\ \Delta_{ij} & -t_{ij} + \mu\delta_{ij} \end{pmatrix} \begin{pmatrix} c_{j\uparrow} \\ c^\dagger_{j\downarrow} \end{pmatrix}. \tag{1.15}$$

Here $c_{i\sigma}$ is the annihilation operator for an electron with spin σ on site i of a square lattice (lattice constant a), the t_{ij}'s are hopping matrix elements, μ is the Fermi energy, and Δ_{ij} is the d-wave pair potential.

Upon particle-hole transformation $d_\uparrow = c_\uparrow$, $d_\downarrow = c^\dagger_\downarrow$, rotation of operators $(d_\uparrow, d_\downarrow) \equiv d \mapsto \exp(i\pi\sigma_x/4)d$, and Fourier transformation the

Hamiltonian becomes:

$$H = \sum_k d^\dagger \left[(t(\boldsymbol{k}) - \mu)\sigma_y + \Delta(\boldsymbol{k})\sigma_x \right] d, \tag{1.16}$$

with $t(\boldsymbol{k}) = t_0[\cos(k_x a) + \cos(k_y a)]$ and $\Delta(\boldsymbol{k}) = \Delta_0[\cos(k_x a) - \cos(k_y a)]$.

For a half-filled band, the superconducting gap closes at the Fermi level in four points, namely at $(k_x, k_y) = (\pm\pi/2a, \pm\pi/2a)$. Expansion near these four nodal points, $k_x = \pm\pi/2a + \delta k_x$, $k_y = \pm\pi/2a + \delta k_y$, gives the linear dispersion relation

$$E = \pm a\sqrt{t_0^2(\delta k_x + \delta k_y)^2 + \Delta_0^2(\delta k_x - \delta k_y)^2}. \tag{1.17}$$

The linearized Hamiltonian takes the form, after rotation by $\pi/4 + \pi n/2$, of an anisotropic Dirac Hamiltonian,

$$\mathcal{H} = \hbar v_F \begin{pmatrix} 0 & \delta k_x - i(\Delta_0/t_0)\delta k_y \\ \delta k_x + i(\Delta_0/t_0)\delta k_y & 0 \end{pmatrix}, \tag{1.18}$$

with $v_F = at_0/\hbar$. The anisotropy is typically large, $\Delta_0/t_0 \simeq 0.07$ in the cuprate superconductor $YBa_2Cu_3O_{7-\epsilon}$.

Electrostatic potential fluctuations move the location of the nodal points, thereby shifting the vector $\delta\boldsymbol{k} \mapsto \delta\boldsymbol{k} + \boldsymbol{A}$ by some offset vector $\boldsymbol{A}$. If the potential varies slowly on the scale of $1/a$, different nodal points remain uncoupled and we may fully account for the potential fluctuations by the effect on each node separately. The slowly varying function $\boldsymbol{A}(\boldsymbol{r})$ then enters into the Dirac equation as a fictitious vector potential.

1.3.3 Dirac fermions in chiral *p*-wave superconductors

The chiral p-wave superconductor Sr_2RuO_4 is a two-dimensional layered structure in the $x-y$ plane. The vector $\boldsymbol{d}_0$ in Eq. (1.14) is oriented along the perpendicular z-direction in zero magnetic field, which implies the antiparallel-spin-triplet pairing $|\uparrow\downarrow\rangle + |\downarrow\uparrow\rangle$. In a perpendicular magnetic field, it is energetically more favorable for $\boldsymbol{d}_0$ to lie in the $x-y$ plane, where it can rotate freely. This implies equal-spin pairing, with decoupled pairs $|\uparrow\uparrow\rangle$ and $|\downarrow\downarrow\rangle$.

Chiral p-wave superconductors with equal-spin pairing can be in two topologically distinct phases, distinguished by the sign of the mass term

in the Dirac equation [122]. To see how this arises, we start from the pairing Hamiltonian

$$H = \sum_{\boldsymbol{k}} \left[\xi_k c_{\boldsymbol{k}}^\dagger c_{\boldsymbol{k}} + \tfrac{1}{2}(\Delta_{\boldsymbol{k}}^* c_{-\boldsymbol{k}} c_{\boldsymbol{k}} + \Delta_{\boldsymbol{k}} c_{\boldsymbol{k}}^\dagger c_{-\boldsymbol{k}}^\dagger) \right]. \tag{1.19}$$

The operator $c_{\boldsymbol{k}}$ is the fermionic annihilation operator (wave vector $\boldsymbol{k}$, spin omitted). We denote by $\xi_k = \hbar^2 k^2/2m - \mu$ the single-particle kinetic energy (relative to the Fermi energy μ). The pair potential has the chiral p-wave form

$$\Delta_{\boldsymbol{k}} = (\Delta_0/k_F)(k_x - ik_y), \tag{1.20}$$

where we have chosen a specific chirality.

The Hamiltonian (1.19) is diagonalized, $H = \sum_{\boldsymbol{k}} \alpha_{\boldsymbol{k}}^\dagger \alpha_{\boldsymbol{k}} + \text{constant}$, via a Bogoliubov transformation,

$$\alpha_{\boldsymbol{k}} = u_{\boldsymbol{k}} c_{\boldsymbol{k}} - v_{\boldsymbol{k}} c_{-\boldsymbol{k}}^\dagger, \quad \alpha_{\boldsymbol{k}}^\dagger = u_{\boldsymbol{k}}^* c_{\boldsymbol{k}}^\dagger - v_{\boldsymbol{k}}^* c_{-\boldsymbol{k}}. \tag{1.21}$$

The electron and hole wave amplitudes $u_{\boldsymbol{k}}$ and $v_{\boldsymbol{k}}$ satisfy the Bogoliubov-De Gennes equations,

$$E_k u_{\boldsymbol{k}} = \xi_k u_{\boldsymbol{k}} - \Delta_{\boldsymbol{k}}^* v_{\boldsymbol{k}}, \quad E_k v_{\boldsymbol{k}} = -\xi_k v_{\boldsymbol{k}} - \Delta_{\boldsymbol{k}} u_{\boldsymbol{k}}. \tag{1.22}$$

Upon substitution of Eq. (1.20), we see that the electron-hole wave function $\psi = (u, v)$ is an eigenstate of the Hamiltonian

$$\begin{aligned} H &= \begin{pmatrix} \xi_k & (\Delta_0/k_F)(-k_x - ik_y) \\ (\Delta_0/k_F)(-k_x + ik_y) & -\xi_k \end{pmatrix} \\ &= \xi_k \sigma_z + (\Delta_0/k_F)(-k_x \sigma_x + k_y \sigma_y), \end{aligned} \tag{1.23}$$

which is a Dirac Hamiltonian with a k-dependent mass ξ_k.

At low energies, $k \to 0$ and we may approximate $\xi_k \approx -\mu$. The sign of μ is a topological invariant, in the sense that it cannot change without closing the excitation gap in the system. Superconductors have typically $\mu > 0$, so a negative mass in the Dirac equation. This is the socalled weak-pairing state. (The strong-pairing state with $\mu < 0$ and positive mass can appear in superfluids [122].)

Electrostatic potential fluctuations cause fluctuations in μ and hence in the mass of the Dirac fermions in the chiral p-wave superconductor. This is in contrast to what we saw in the previous subsection for the d-wave superconductor, where electrostatic potential fluctuations appear as a vector potential for the Dirac fermions.

1.4 Majorana fermions

The Bogoliubov-De Gennes equations (1.22) have particle-hole symmetry, such that if $\big(u(\boldsymbol{r}), v(\boldsymbol{r})\big)$ is an eigenstate at energy E then $(v^*(\boldsymbol{r}), u^*(\boldsymbol{r}))$ is an eigenstate at energy $-E$. (We work in real space, with $\boldsymbol{k} = -i\partial/\partial\boldsymbol{r}$.) In terms of the quasiparticle annihilation operator $\alpha(E)$ of an eigenstate at energy E, this symmetry relation reads $\alpha(E) = \alpha^\dagger(-E)$. At zero excitation energy, $\alpha = \alpha^\dagger$, so the excitation is a Majorana fermion (particle equal to antiparticle). Because zero energy is measured relative to the Fermi level, at the center of the excitation gap, such Majorana bound states are midgap states.

Chiral p-wave superconductors can have Majorana bound states, trapped inside the normal core of a magnetic vortex [122]. A vortex in a conventional s-wave superconductor also traps states inside the gap, but these are displaced from $E = 0$ by the energy Δ_0^2/E_F of zero-point motion, so they are not midgap states.

Because the Majorana bound states are all at the same energy, tunneling from one vortex to the other is a resonant process. For a sufficient density of vortices the wave functions extend throughout the system, rather than being localized inside the vortices. The superconductor is then a *thermal metal* rather than a *thermal insulator*. The adjective "thermal" is added because the excitations in a superconductor are charge neutral, so they transport thermal energy but no electrical charge.

One of the findings of our thesis, is that Majorana fermions can be created in chiral p-wave superconductors by a purely electrostatic mechanism, without requiring a magnetic vortex. A change in the sign of the mass $\mu(\boldsymbol{r})$ along a line defect creates Majorana bound states at the two end points.

One might wonder whether this mechanism would be operative also in graphene, if a staggered potential would create a similar line defect. The answer is negative, as we will show later in the thesis, for the following reason: A sign change in the mass will only produce a Majorana bound state if the mass has a nonzero k^2 term. This is the case for the mass term $\xi_k = \hbar^2k^2/2m - \mu$ in the chiral p-wave superconductor Hamiltonian (1.23), but not for the graphene Hamiltonian (1.5).

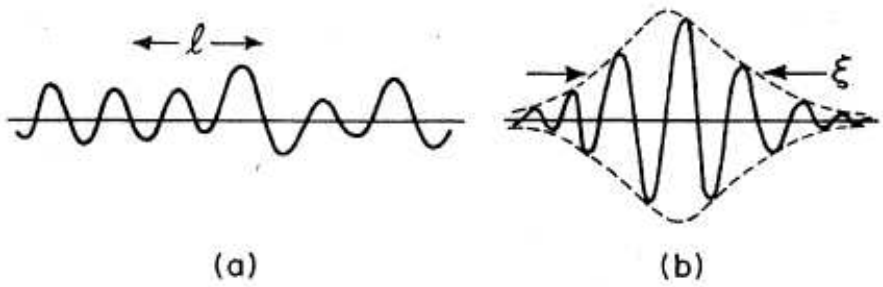

Figure 1.4. Typical wavefunction for a) delocalized and b) localized states, with the mean free path l and the localization length ξ indicated. From Ref. [69].

1.5 Scaling theory of localization

We will study the phase transition from a thermal metal to a thermal insulator within the context of the scaling theory of localization [69]. A summary of that theory is presented here, for the *electrical* metal-insulator transition. We will see later in the thesis what qualitative differences appear for the *thermal* metal-insulator transition.

1.5.1 Single-parameter scaling

The single-parameter scaling hypothesis [1] states that the conductance of a d-dimensional conductor of linear size L depends on the microscopic parameters of the system through a single length scale ξ, called the localization length in the insulator and the correlation length (or mean free path) in the metal. (See Fig. 1.4.) In units of e^2/h, the dimensionless conductance $g = f(L/\xi)$ is therefore a function of the ratio L/ξ. The function f may depend on the dimensionality d and on fundamental symmetries of the system (for example, the presence or absence of time-reversal symmetry), but it may not depend on microscopic parameters (such as the mean free path l).

In a metal, Ohm's law implies that $g \propto L^{d-2}$ depends as a power law on L. In an insulator, the conductance decays exponentially, $g \propto e^{-L/\xi}$. In order to interpolate between these two limits, it is convenient to work with the logarithmic derivative $\beta = d \ln g / d \ln L$. According to single-parameter scaling, $\beta(g)$ can be expressed as a function of g itself. The

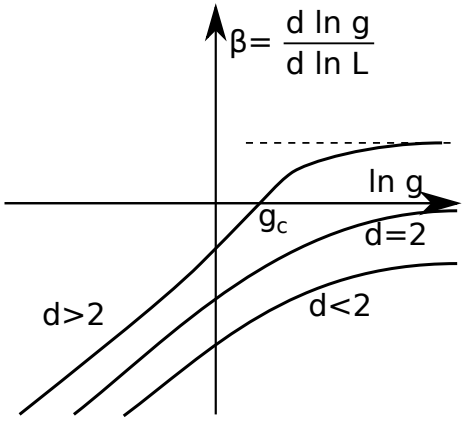

Figure 1.5. Schematic β-function for the electrical metal-insulator transition in different dimensions, in the presence of time-reversal symmetry.

two limits are

$$\beta(g) = \ln(g/g_c), \tag{1.24}$$

in an insulator and

$$\beta(g) = d - 2 + \delta(g), \tag{1.25}$$

in a metal. The first quantum correction to Ohm's law, $\delta(g) = a/g$ with $a < 0$, can be calculated by perturbation theory.

The β-function for the electrical metal-insulator transition is shown in Fig. 1.5, for different dimensions and in the presence of time-reversal symmetry [1]. (We also assumed that spin is a conserved quantity.) For $d = 3$ there is a critical point g_c where the β-function equals zero, meaning that the conductance of the system is scale invariant (independent of L). This fixed point signals the metal-insulator transition. It is an unstable fixed point, since on one side the system scales to a metal and on the other side to an insulator.

1.5.2 Critical exponent

The critical exponent ν quantifies how unstable the fixed point is. Let us assume that $1/\nu$ is the slope of the β-function at g_c, with $\beta(g_c) = 0$. Integration of $\beta(g) = d \ln g / d \ln L$ from the metallic side gives

$$\ln \frac{g}{g_c} = \left(\frac{L}{\lambda}\right)^{1/\nu} \ln \frac{g_\lambda}{g_c}, \tag{1.26}$$

where (λ, g_λ) is some point on the scaling curve in the vicinity of g_c with $\beta(g_\lambda) > 0$. Integration from the insulating side gives

$$g \sim g_c \exp(-BL\delta g^\nu/\lambda), \tag{1.27}$$

with B a constant and $\delta g = g_c - g$.

In the metallic regime the point $\beta(g_\xi) = 1$ is determined by the correlation length

$$\xi = \lambda \left(\frac{1}{\nu} \ln \frac{g_\lambda}{g_c}\right)^{-\nu}. \tag{1.28}$$

The correlation length (or mean free path) is the minimal length when Ohm's law is applicable. In the insulating regime the localization length ξ following from the definition $g = g_c \exp(-L/\xi)$ is

$$\xi = \frac{\lambda}{B\delta g^\nu}. \tag{1.29}$$

1.5.3 Finite-size scaling

The hypothesis of single-parameter scaling holds in the large-L limit. For finite L corrections appear, which one needs to take into account in order to reliably determine the critical conductance and critical exponent [65].

Let us consider a finite system which is characterized by several parameters $\{x_i\}$, for example, mean free path, electron density, etc. We consider the L dependence of a variable F which becomes scale invariant at the metal-insulator transition. Typically, F is the conductance, but other quantities can be useful in computer simulations.

According to the scaling hypothesis, the function $F_L = F(\{x_i\}, L)$ can be written in the form

$$F_L = F(\chi L^{1/\nu}, \phi_1 L^{y_1}, \phi_2 L^{y_2}, \dots), \tag{1.30}$$

with $\nu > 0$ the critical exponent and all $y_i < 0$. So in the large-L limit the terms with y_i die out and the parameters ϕ_i become irrelevant.

Near the phase transition χ as a function of a control parameter x can be expanded as

$$\chi = \chi_1(x - x_c) + \chi_2(x - x_c)^2 + \dots. \tag{1.31}$$

The vanishing of χ at the phase transition x_c implies that F becomes scale invariant in the large-L limit.

1.5.4 Symmetry classes

The electrical metal-insulator transition discussed so far, with the scaling function shown in Fig. 1.5, holds for electrons described by the Schrödinger equation, in the presence of time-reversal symmetry and spin-rotation symmetry. This symmetry class is denoted as AI. (The name comes from the mathematics literature.)

The thermal metal-insulator transition in a chiral p-wave superconductor is in a different universality class: The excitations are described by a Dirac equation, with time-reversal symmetry and spin-rotation symmetry both broken, but with an additional symmetry, which is particle-hole symmetry. This symmetry class is denoted as BD or D (depending on whether or not there is vortex disorder).

There are in total 10 symmetry classes in the theory of localization, depending on the presence or absence of time-reversal symmetry, spin-rotation symmetry, particle-hole symmetry, and sublattice (or chiral) symmetry [36]. In this thesis we will be concerned mainly with class BD/D. One other symmetry class will appear for d-wave superconductors, which is class AIII (chiral symmetry without time-reversal symmetry).

The β-function is different in each symmetry class. In particular, in class BD there can be a metal-insulator transition already in two dimensions, which is not possible in class AI. In class AIII there is no insulating phase at all.

1.6 Dirac fermions on a lattice

Our numerical studies of localization of Dirac fermions are based on a transfer matrix discretization of the Dirac equation, either in real space or in momentum space. We will introduce the different discretization schemes in this section.

An alternative approach, which we have not taken, is based on models which are in the same universality class D as the Dirac equation, but which do not approach the Dirac equation in the continuum limit [36]. These generic class D models are variations of the Chalker-Coddington network model [24]. Our preference for a discretization of the Dirac equation is that we can stay closer to a specific physical system (graphene or a chiral p-wave superconductor) and have direct access to a physical

observable (electrical or thermal conductance).

One obvious requirement of any discretization is that it should preserve Hermiticity of the Hamiltonian. In a transfer matrix formulation this requirement appears as the requirement of current conservation. Two further requirements are special for Dirac fermions: we should avoid fermion doubling and preserve symplectic symmetry.

1.6.1 Avoid fermion doubling

Dirac fermions on a lattice were introduced in the context of QCD [100]. It was discovered in that context that a straightforward discretization of the Dirac equation introduces a spurious second Dirac point in the spectrum. This is the notorious fermion doubling problem.

A simple one-dimensional discretization shows the nature of the problem. Let us assume that there is a lattice with lattice spacing a and number of lattice points N. We want to discretize on it the equation

$$-i\partial_x \psi(x) = \lambda \psi(x). \tag{1.32}$$

Notice that the spectrum of the continuous equation is $\lambda(k) = k$. A naive discretization of the derivative,

$$\partial_x \psi(x) \longrightarrow \frac{\psi(x+a) - \psi(x)}{a}, \tag{1.33}$$

does not produce a Hermitian operator $-i\partial_x \psi$ on the lattice. There is a simple way to make it Hermitian, namely by symmetrization,

$$\partial_x \psi(x) \longrightarrow \frac{\psi(x+a) - \psi(x-a)}{2a}. \tag{1.34}$$

Fourier transformation, $\psi(x) = \sum_p \exp(ipx)\psi(p)$ with $p = 2\pi m/aN$, $m = 1, 2, \ldots, N$, gives the spectrum

$$\lambda(p) = \sin(pa)/a. \tag{1.35}$$

Near $p = 0$ we recover the linear spectrum of the continuous equation (1.32). The derivative $\partial\lambda/\partial p > 0$ near $p = 0$, so the particles are right-moving. But in the vicinity of $p = \pi/a$ there is one more zero in the dispersion relation (see Fig. 1.6), with $\partial\lambda/\partial p < 0$, so a second species of left-moving particles has appeared — which is not present in the continuous equation.

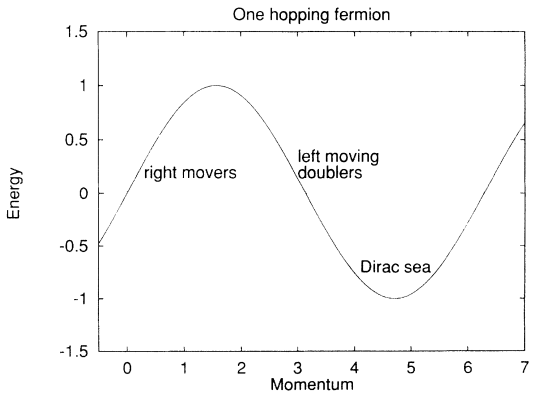

Figure 1.6. Illustration of fermion doubling in one dimension. From Ref. [30].

The Nielsen-Ninomiya "no-go" theorem [85] states that fermion doubling (with an equal number of left-movers and right-movers) is unavoidable for a discretization scheme which is Hermitian, local, and translationally invariant. The reason is that periodicity in lattice momentum p gives an equal number of zeros with positive and negative slopes.

If some of the conditions of the theorem are not met, then it is possible to avoid fermion doubling. The transfer matrix discretization schemes that we will use in this thesis (in real space and momentum space) are nonlocal. This complicates the algorithm, but it has the great advantage that it preserves the symplectic symmetry of the Dirac equation. An alternative approach is to make one of the two fermion species massive (Wilson fermion). This produces an easier algorithm, but breaks symplectic symmetry.

1.6.2 Conserve current and preserve symmetries

The transfer matrix of the Dirac Hamiltonian

$$H = v_F(p_x\sigma_x + p_y\sigma_y) + m(\boldsymbol{r})v_F^2\sigma_z + u(\boldsymbol{r}), \tag{1.36}$$

can be calculated by integrating the eigenvalue equation $H\Psi = E\Psi$ in the form

$$\partial_x\Psi = \Big[-ip_y\sigma_z/\hbar - iU(\boldsymbol{r})\sigma_x - M(\boldsymbol{r})\sigma_y\Big]\Psi, \tag{1.37}$$

with $U = (u - E)/\hbar v_F$ and $M = mv_F/\hbar$.

For this integration we discretize a rectangular strip on an $M \times N$ lattice, with M columns in the x-direction and N rows in the y-direction. We take periodic boundary conditions in the y-direction. The values $\Psi_{m,n} = \Psi(x_m, y_n)$ of the wave function at a lattice point are collected into a set vectors $\mathbf{\Psi}_m$. The transfer matrix $\mathcal{T}_m$ of slice m is defined by

$$\mathbf{\Psi}_{m+1} = \mathcal{T}_m \mathbf{\Psi}_m. \tag{1.38}$$

The transfer matrix $\mathcal{T}$ through the entire strip is then the product of the $\mathcal{T}_m$'s.

Current conservation, with current operator $\mathcal{J}_x$ along the strip, requires that

$$\langle \Psi_1 | \mathcal{J}_x | \Psi_1 \rangle = \langle \Psi_M | \mathcal{J}_x | \Psi_M \rangle \Rightarrow \mathcal{J}_x = \mathcal{T}^\dagger \mathcal{J}_x \mathcal{T}. \tag{1.39}$$

Preservation of symplectic symmetry imposes an additional condition on the transfer matrix. Symplectic symmetry is the invariance of the Hamiltonian under inversion of momentum and spin. It is broken by a mass term, so this is not an important requirement if one studies, for example, gapped graphene.

For massless Dirac fermions in a scalar potential u the Hamiltonian $H = v_F \boldsymbol{p} \cdot \boldsymbol{\sigma} + u(\boldsymbol{r})$ is invariant under inversion $\boldsymbol{p} \mapsto -\boldsymbol{p}$, $\boldsymbol{\sigma} \mapsto -\boldsymbol{\sigma}$. This symmetry can equivalently be written as $H = \sigma_y H^* \sigma_y$, where the complex conjugation is carried out in the real space basis (when $\boldsymbol{p} = -i\hbar\partial/\partial\boldsymbol{r}$). The condition on the transfer matrix is

$$\mathcal{T} = \sigma_y \mathcal{T}^* \sigma_y. \tag{1.40}$$

The Dirac Hamiltonian $H = v_F(p_x\sigma_x + p_y\sigma_y) + mv_F^2\sigma_z$ with a mass term, but without the scalar potential, has no symplectic symmetry but instead has particle-hole symmetry: $\sigma_x H^* \sigma_x = -H$. This is the relevant Hamiltonian for a chiral p-wave superconductor. The corresponding symmetry relation for the transfer matrix is

$$\mathcal{T}(E) = \sigma_x \mathcal{T}^*(-E)\sigma_x. \tag{1.41}$$

1.6.3 Real space discretization

The transfer matrix resulting from the real space discretization of Eq. (1.37) was calculated in Ref. [119], using the staggered fermion approach from QCD [100]. We summarize this method.

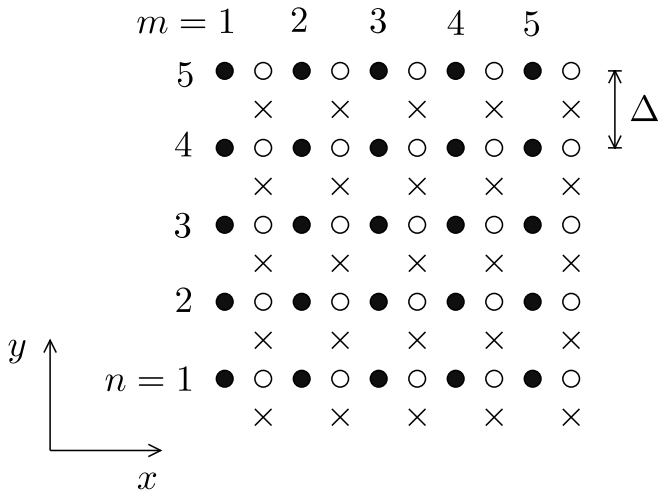

Figure 1.7. Square lattice (filled circles) on which the wave function Ψ is discretized as $\Psi_{m,n}$. The finite differences are evaluated at the displaced points indicated by crosses. The Dirac equation (1.37) is applied at the empty circles, by taking the mean of the contributions from the two adjacent crosses. From Ref. [119].

Discretized operators are defined at points of the displaced lattice shown in Fig. 1.7. The differential operators are discretized by

$$\partial_x \Psi \to \frac{1}{2a}(\Psi_{m+1,n} + \Psi_{m+1,n+1} - \Psi_{m,n} - \Psi_{m,n+1}), \tag{1.42}$$

$$\partial_y \Psi \to \frac{1}{2a}(\Psi_{m,n+1} + \Psi_{m+1,n+1} - \Psi_{m,n} - \Psi_{m+1,n}). \tag{1.43}$$

The potential and mass terms are replaced by averages over adjacent lattice points,

$$M\sigma_z \Psi \to \quad \tfrac{1}{4} M_{m,n}\sigma_z \big(\Psi_{m+1,n} + \Psi_{m+1,n+1} + \Psi_{m,n} + \Psi_{m,n+1}\big), \tag{1.44}$$

$$U\Psi \to \quad \tfrac{1}{4} U_{m,n} \big(\Psi_{m+1,n} + \Psi_{m+1,n+1} + \Psi_{m,n} + \Psi_{m,n+1}\big), \tag{1.45}$$

with $M_{m,n} = M(x_m + a/2, y_n + a/2)$ and $U_{m,n} = U(x_m + a/2, y_n + a/2)$.

The zero-energy Dirac equation $H\Psi = 0$ is applied at the points $(x_m + a/2, y_n)$ by averaging the terms at the two adjacent points $(x_m + a/2, y_n \pm a/2)$. The resulting finite difference equation can be written in a compact form with the help of the $N_y \times N_y$ tridiagonal matrices $\mathcal{J}$, $\mathcal{K}$,

$\mathcal{M}^{(m)}$, defined by the following nonzero elements:

$$\mathcal{J}_{n,n} = 1, \;\; \mathcal{J}_{n,n+1} = \mathcal{J}_{n,n-1} = \tfrac{1}{2}, \tag{1.46}$$

$$\mathcal{K}_{n,n+1} = \tfrac{1}{2}, \;\; \mathcal{K}_{n,n-1} = -\tfrac{1}{2}, \tag{1.47}$$

$$\mathcal{M}^{(m)}_{n,n} = \tfrac{1}{2}(M_{m,n} + M_{m,n-1}), \;\; \mathcal{M}^{(m)}_{n,n+1} = \tfrac{1}{2}M_{m,n}, \mathcal{M}^{(m)}_{n,n-1} = \tfrac{1}{2}M_{m,n-1}, \tag{1.48}$$

$$\mathcal{V}^{(m)}_{n,n} = \tfrac{1}{2}(U_{m,n} + U_{m,n-1}), \;\; \mathcal{U}^{(m)}_{n,n+1} = \tfrac{1}{2}U_{m,n}, \mathcal{U}^{(m)}_{n,n-1} = \tfrac{1}{2}U_{m,n-1}. \tag{1.49}$$

In accordance with the periodic boundary conditions in the transverse direction, the indices $n \pm 1$ should be evaluated modulo N_y.

The discretized Dirac equation is expressed in terms of the matrices (1.46)–(1.49) by

$$\frac{1}{2a}\mathcal{J}(\mathbf{\Psi}_{m+1} - \mathbf{\Psi}_m) = \left(-\frac{i}{2a}\sigma_z\mathcal{K} - \frac{1}{4}v^2\sigma_y\mathcal{M}^{(m)} - \frac{i}{4}v^2\sigma_x\mathcal{V}^{(m)}\right)(\mathbf{\Psi}_m + \mathbf{\Psi}_{m+1}). \tag{1.50}$$

Rearranging Eq. (1.50) we arrive at Eq. (1.38) with the transfer matrix

$$\mathcal{T}_m = \left(\mathcal{J} + i\sigma_z\mathcal{K} + \tfrac{1}{2}v^2a\sigma_y\mathcal{M}^{(m)}\right)^{-1}\left(\mathcal{J} - i\sigma_z\mathcal{K} - \tfrac{1}{2}v^2a\sigma_y\mathcal{M}^{(m)}\right). \tag{1.51}$$

For a uniform mass $M_{mn} = M$ and uniform potential $U_{mn} = \epsilon$, we may calculate the eigenvalues e^{ik_xa} of $\mathcal{T}_m$ analytically. This gives the dispersion relation

$$\tan^2(k_xa/2) + \tan^2(k_ya/2) + (Mav_F/2\hbar)^2 = (\epsilon/2)^2, \tag{1.52}$$

with $k_y = 2\pi l/N_y$, $l = 1, 2, \ldots N_y$. The zero of the dispersion relation at $k_x = \pi/a$, responsible for the fermion doubling, is replaced by a pole. The nonlocality of the staggered discretization scheme works around the no-go theorem.

This discretization scheme conserves the current operator

$$J_x = \tfrac{1}{2}v\sigma_x\mathcal{J}. \tag{1.53}$$

It preserves symplectic symmetry for $M = 0$ and obeys particle-hole symmetry for $U = 0$.

1.6.4 Momentum space discretization

An alternative momentum space discretization was developed in Ref. [11]. The differential equation (1.37) is integrated in the x-direction by a straightforward discretization in real space, but in the y-direction the discretization of p_y is carried out in momentum space. The combination of these two discretizations produces a nonlocal transfer matrix, which works around the no-go theorem for fermion doubling, preserving current and all symmetries.

The algorithm is simplified by carrying out the two discretizations in separate steps. One step accounts for scattering $\mathcal{S}$ by disorder in a single slice, another step accounts for free propagation $\mathcal{P}$ from one slice to the next:

$$\mathcal{S}_m = \exp(-iU_m\sigma_x - M_m\sigma_y), \tag{1.54}$$

$$\mathcal{P} = \exp(-ip_y\sigma_z a/\hbar). \tag{1.55}$$

Here U_m and M_m are diagonal matrices containing the potential and mass at column m on the diagonal.

The transfer matrix is the product

$$\mathcal{T} = \mathcal{P}\mathcal{U}\mathcal{S}_M\mathcal{U}^\dagger\mathcal{P}\mathcal{U}\cdots\mathcal{S}_2\mathcal{U}^\dagger\mathcal{P}\mathcal{U}\mathcal{S}_1\mathcal{U}^\dagger\mathcal{P}, \tag{1.56}$$

with $\mathcal{U}$ the matrix that Fourier transforms from real space to momentum space. The size of this matrix is made finite by truncating the transverse momentum p_y at some large value.

1.7 This thesis

We summarize the contents of the following chapters.

1.7.1 Chapter 2

This chapter is a numerical study of quasiparticle localization in symmetry class BD (realized, for example, in chiral p-wave superconductors), by means of a staggered-fermion lattice model for two-dimensional Dirac fermions with a random mass. For sufficiently weak disorder, the system size dependence of the average (thermal) conductivity σ is well described by an effective mass $M_{\rm eff}$, dependent on the first two moments of the random mass $M(\boldsymbol{r})$. The effective mass vanishes linearly when the

average mass $\bar{M} \to 0$, reproducing the known insulator-insulator phase boundary with a scale invariant dimensionless conductivity $\sigma_c = 1/\pi$ and critical exponent $\nu = 1$. For strong disorder a transition to a metallic phase appears, with larger σ_c but the same ν. The intersection of the metal-insulator and insulator-insulator phase boundaries is identified as a *repulsive* tricritical point.

1.7.2 Chapter 3

In this chapter we look at quasiparticle localization in symmetry class *D*. It is different from class *BD* by absence of the bound states at zero energy. The system is modeled by staggered fermions in momentum space and uses convergence in momentum space to realize a smooth potential landscape in real space. Graphene with a random gap in a known realization of such system. It is known that fluctuations in the electrostatic potential allow for metallic conduction (nonzero conductivity in the limit of an infinite system) if the carriers form a single species of massless two-dimensional Dirac fermions. A nonzero uniform mass $\bar{M}$ opens up an excitation gap, localizing all states at the Dirac point of charge neutrality. Here we investigate numerically whether fluctuations $\delta M \gg \bar{M} \neq 0$ in the mass can have a similar effect as potential fluctuations, allowing for metallic conduction at the Dirac point. Our negative conclusion confirms earlier expectations, but does not support the recently predicted metallic phase in a random-gap model of graphene [131].

1.7.3 Chapter 4

Vortices in two-dimensional superconductors with broken time-reversal and spin-rotation symmetry can bind states at zero excitation energy. These socalled Majorana bound states transform a thermal insulator into a thermal metal and may be used to encode topologically protected qubits. We identify an alternative mechanism for the formation of Majorana bound states, akin to the way in which Shockley states are formed on metal surfaces: *An electrostatic line defect can have a pair of Majorana bound states at the end points.* The Shockley mechanism explains the appearance of a thermal metal in vortex-free lattice models of chiral *p*-wave superconductors and (unlike the vortex mechanism) is also operative in the topologically trivial phase.

1.7.4 Chapter 5

The bulk microwave conductivity of a dirty d-wave superconductor is known to depend sensitively on the range of the disorder potential: long-range scattering enhances the conductivity, while short-range scattering has no effect. In this chapter we show that the three-terminal electrical conductance of a normal-metal–d-wave superconductor–normal-metal junction has a dual behavior: short-range scattering suppresses the conductance, while long-range scattering has no effect.

1.7.5 Chapter 6

In this chapter we investigate nanomechanical properties, namely the conductivity of a clean graphene sheet, deformed by a gate electrode. The effect of the deformation on the conductivity is twofold: The lattice distortion can be represented as a pseudovector potential in the Dirac equation, whereas the gate causes a inhomogeneous density redistribution. We use elasticity theory to find the profile of the graphene sheet and then evaluate the conductivity by means of the transfer matrix approach. We find that the two effects provide qualitatively different contributions to the conductivity. For small deformations and not too high residual stress the correction due to the charge redistribution dominates and leads to the enhancement of the conductivity. For stronger deformations, the effect of the lattice distortion becomes more important and eventually leads to the suppression of the conductivity. We consider homogeneous as well as local deformation. We also suggest that the effect of the charge redistribution can be best measured in a setup containing two gates, one fixing the overall charge density and another one deforming graphene locally.